Hindawi Publishing Corporation
Journal of Nanomaterials
Volume 2015, Article ID 373675, 7 pages
http://dx.doi.org/10.1155/2015/373675

Hindawi

Research Article

A Comparative Study of Er^{3+}, Er^{3+}-Eu^{3+}, Er^{3+}-Tb^{3+}, and Er^{3+}-Eu^{3+}-Tb^{3+} Codoped Y_2O_3 Nanoparticles as Optical Heaters

G. A. Sobral Jr.,[1] M. A. Gomes,[2] J. F. M. Avila,[2] J. J. Rodrigues Jr.,[2] Z. S. Macedo,[2] and M. A. R. C. Alencar[2]

[1]*Programa de Pós-Graduação em Materiais, Universidade Federal de Alagoas, 57072-970 Maceió, AL, Brazil*
[2]*Departamento de Física, Universidade Federal de Sergipe, Cidade Universitária Prof. José Aloísio de Campos, Rodovia Marechal Rondon s/n, Jardim Rosa Elze, 57072-970 São Cristóvão, SE, Brazil*

Correspondence should be addressed to M. A. R. C. Alencar; marca@optma.org

Received 27 August 2015; Revised 13 November 2015; Accepted 15 November 2015

Academic Editor: Piaoping Yang

Fluorescence intensity ratio (FIR) technique, based on the thermal coupling of $^2H_{11/2}$ and $^4S_{3/2}$ energy levels of erbium ions, was used to study the optical heating behavior of rare earth doped yttrium oxide nanophosphors (Y_2O_3:Er^{3+}, Y_2O_3:Er^{3+}-Eu^{3+}, Y_2O_3:Er^{3+}-Tb^{3+}, and Y_2O_3:Er^{3+}-Eu^{3+}-Tb^{3+}) synthesized via PVA-assisted sol-gel route. The samples were optically heated by an 800 nm CW diode laser, while the upconverted green emissions were used to measure their temperatures in real time. The experimental results indicate that the studied nanoparticles are promising candidates to applications such as photothermal treatments and hyperthermia.

1. Introduction

Since the discovery that biological tissues are permeable to NIR radiation, characterizing what became known as optical biological windows [1, 2], several studies have been done in order to explore bioapplications involving this spectral region [3]. In particular, the branch of the nanocrystals doped with rare earth ions proved to be quite versatile for this purpose. For example, the phenomenon of frequency upconversion under NIR excitation that occurs in several rare earth ions has proved to be effective for bioimaging applications and temperature sensing with high spatial resolution [4, 5]. More recently, several studies have demonstrated the possibility of using such particles as optical nanoheaters and proposed their use in cancer therapy based on hyperthermia [6–8].

In this emerging field of study, we highlight the nanocrystals which use ytterbium as sensitizer [9, 10], since the doping with this ion increases significantly the efficiency of fluorescent processes. However, the particles' excitation is restricted to the region around 980 nm, where ytterbium has its single excitation band. This is the same optical region where water has high absorption, which reduces the effectiveness of the process for biological applications [11]. As an alternative, nanocrystals doped with neodymium were already effectively used as nanoheaters and optical sensors with excitation around 800 nm [3, 12], with the advantage that in this spectral region biological tissues are more permeable to NIR radiation [13]. Nevertheless, considering the wide variety of rare earth ions, the number of proposals exploring this excitation region is still small.

In this paper, we examine the influence of different doping (Er^{3+}, Eu^{3+}, and Tb^{3+}) over the optical heating behavior and temperature sensing of Y_2O_3 nanoparticles, excited by an 800 nm CW diode laser. To estimate the temperature of the nanoparticles, FIR technique based on the upconverting green emissions of Er^{3+} ions was used. To the best of our knowledge, there is no report about the optical heating behavior of rare earth doped Y_2O_3 nanoparticles under 800 nm CW laser excitation. In our study, the temperatures reached by the particles, as well as the power densities used, are in the regions commonly used for hyperthermia treatments [14], making these nanoparticles promising candidates for this kind of application.

2. Methods

The samples were produced via PVA-assisted sol-gel route, employing $Y(NO_3)_3$, $ErCl_3{\cdot}6H_2O$, $TbCl_3{\cdot}6H_2O$, and $Eu(NO_3)_3$ (Aldrich, grade purity 99.99% or higher) as precursors. For the Y_2O_3:Er^{3+}, Y_2O_3:Er^{3+}-Eu^{3+}, Y_2O_3:Er^{3+}-Tb^{3+}, and Y_2O_3:Er^{3+}-Eu^{3+}-Tb^{3+} samples, each dopant concentration was fixed at 1 mol%. The starting materials were dissolved in distilled water in a concentration of 0.2 g/mL. After that, a 10% (w/v) aqueous solution of PVA was added to the starting solution under continuous stirring at room temperature. After 30 min stirring, the material was dried at 100°C for 24 h, then kept at 200°C for 5 h, and finally calcined at 1000°C for 5 h.

The crystalline phase of the powders was inspected by X-ray diffraction (XRD, Rigaku RINT 2000/PC), while morphology and particle size of the samples were analyzed by scanning electron microscopy (SEM) using a Jeol JSM5500F equipment.

All upconversion (UC) luminescence spectra measurements were performed using a set of lenses for fluorescence collection and an optical fiber connected to an Ocean Optics USB4000 spectrometer with samples being excited by an 800 nm CW diode laser. During these measurements, size and shape of the spot on the samples were kept fixed (elliptical shape with main axes of 1.5 mm and 0.75 mm). On the temperature sensing calibration process, the samples were kept over an adjustable electric hotplate with a thermocouple placed 2 mm apart from the focal spot to temperature recording. To avoid a significant optical heating of the samples during this process, the laser pump power was set to 110 mW (12.4 W/cm^2 power density). For the measurements using increasing pump power densities, the laser power was adjusted from 211 mW to 1200 mW.

3. Results and Discussion

3.1. Structure and Morphology of the Synthesized Material. Figure 1 presents XRD pattern of Y_2O_3:Er^{3+}-Eu^{3+}-Tb^{3+} after calcination at 1000°C for 5 h. For all the samples studied, the obtained XRD patterns were consistent with single phase Y_2O_3 (ICSD card #086817). The Rietveld refinement of the pattern confirmed a cubic structure and spatial group Ia3.

The crystallite size was estimated from the FWHM of the diffraction peaks using Scherrer's equation $d = K\lambda/\beta \cdot \cos\theta_B$, where K is the shape coefficient for the reciprocal lattice point (in this work $K = 0.89$), l is the wavelength of the X-rays ($l = 0.15405$ nm), q_B is the peak position, and $\beta = \sqrt{B^2 - b^2}$ is the width of specimen's peak (B) corrected by an instrumental broad factor (in this work, $b = 0.005192$ rad) [15, 16]. The average crystallite size was estimated as 43 ± 1 nm for the pattern shown in Figure 1 (sample Y_2O_3:Er^{3+}-Eu^{3+}-Tb^{3+}). The same results were obtained for the other Y_2O_3 samples (pure and doped) produced for this work. Figure 2 presents SEM images for pure and doped Y_2O_3 annealed at 1000°C. The image shows that the particles have homogeneous size distribution with average particle size of about 50 nm, confirming the results obtained from the XRD data.

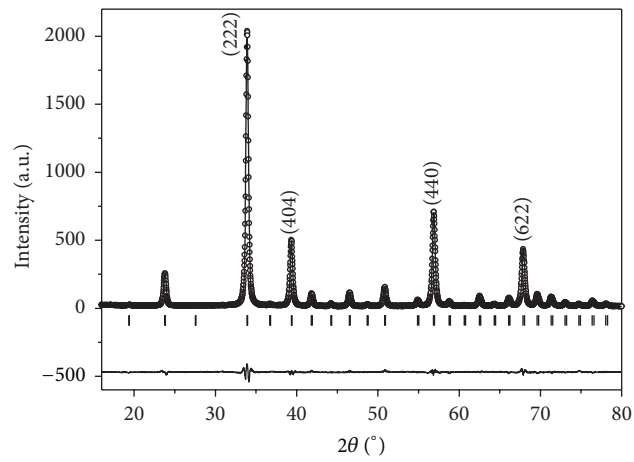

Figure 1: The Rietveld refinement of Y_2O_3:Er^{3+}-Eu^{3+}-Tb^{3+}. Open circles represent the XRD data and the solid curve represents the calculated pattern. Difference plot is shown at the bottom of the graph.

3.2. Temperature Sensing Performance. Figure 3 presents the UC spectra produced by transitions $^2H_{11/2} \rightarrow {}^4I_{15/2}$ and $^4S_{3/2} \rightarrow {}^4I_{15/2}$ of Er^{3+} ions for all studied samples at two extreme temperatures. As can be seen, there is a consistent behavior of the emission spectra for all samples in the analyzed temperature region where, with increasing temperature, the intensity of the band around 523 nm ($^2H_{11/2} \rightarrow {}^4I_{15/2}$) intensifies with respect to the band around 551 nm ($^4S_{3/2} \rightarrow {}^4I_{15/2}$).

Due to the small difference in energy between the emitting levels $^2H_{11/2}$ and $^4S_{3/2}$ (about 770 cm^{-1}) they are thermally coupled [17]; that is, populations of these levels are related to each other by Boltzmann's distribution and, consequently, so do fluorescence intensities produced by these levels. Therefore, a correlation between the fluorescence intensity ratio (FIR) of these levels and the sample's temperature can be expressed by [18]

$$\begin{aligned} \mathrm{FIR} = \frac{I_H}{I_L} &= \frac{c_H(\nu)\, A_H g_H h\nu_H}{c_L(\nu)\, A_L g_L h\nu_L} \exp\left(\frac{-\Delta E}{kT}\right) \\ &= C \exp\left(\frac{-\Delta E}{kT}\right), \end{aligned} \tag{1}$$

where the indexes H and L refer to the higher ($^2H_{11/2}$) and lower ($^4S_{3/2}$) thermally coupled energy levels of erbium, respectively; I_i corresponds to the integrated fluorescence intensity of the emission band; $c_i(\nu_i)$ is a function of the fluorescence collection efficiencies; ν_i refers to the emitted light frequency; A_i is the spontaneous radiative emission rate of each band; g_i corresponds to the level's degeneracy; $h\nu_i$ is the average photon energy of each band; ΔE is the energy gap between the levels $^4S_{3/2}$ and $^2H_{11/2}$; k is Boltzmann's

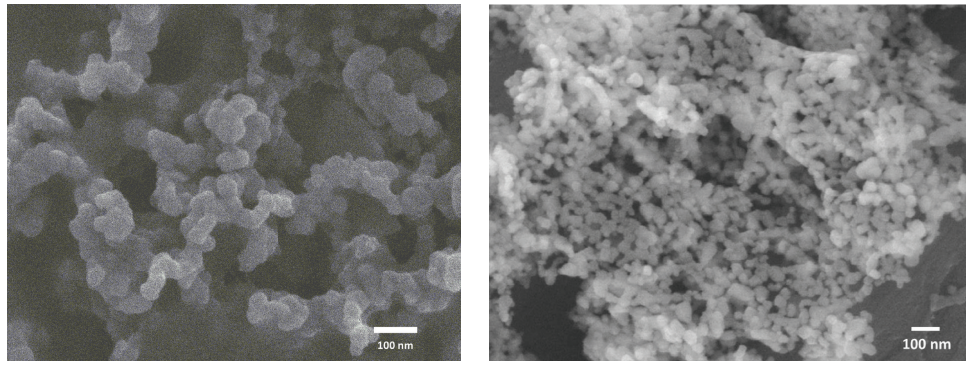

(a) (b)

FIGURE 2: SEM image of Y_2O_3 after calcination at 1000°C/5 h, with average particle size of about 50 nm: (a) pure sample, (b) sample doped with Er^{3+}-Eu^{3+}-Tb^{3+}.

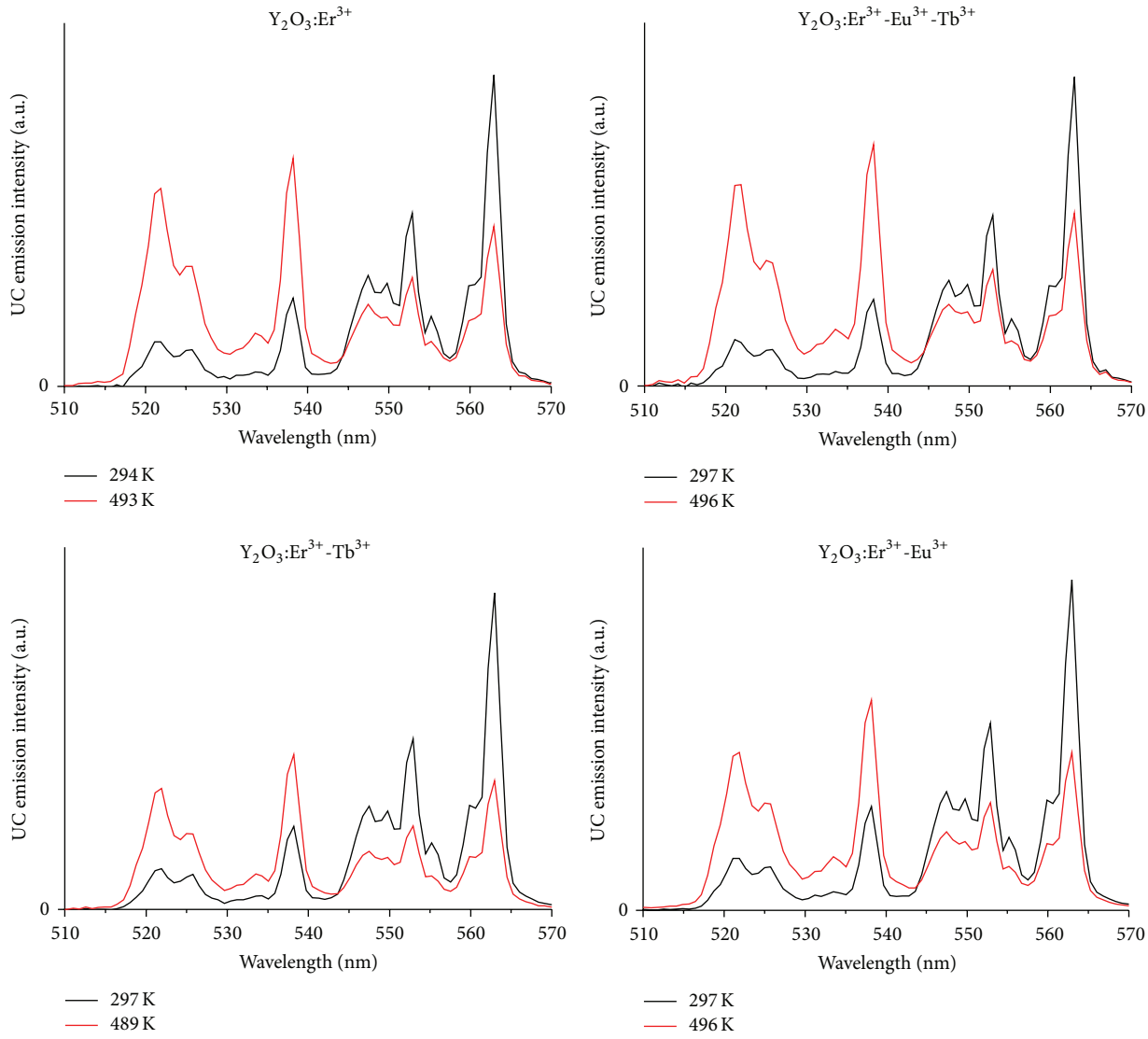

FIGURE 3: Upconversion emission spectra due to $^2H_{11/2} \rightarrow {}^4I_{15/2}$ and $^4S_{3/2} \rightarrow {}^4I_{15/2}$ transitions of Er^{3+} ions for all studied samples at two extreme temperatures.

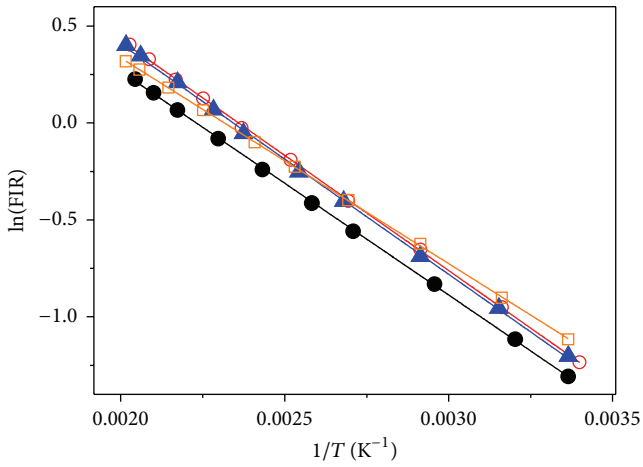

Figure 4: Fluorescence intensity ratio as a function of the inverse of the temperature for the investigated samples, Y_2O_3:Er^{3+} (open red circles), Y_2O_3:Er^{3+}-Tb^{3+} (solid black circles), Y_2O_3:Er^{3+}-Eu^{3+} (open orange squares), and Y_2O_3:Er^{3+}-Eu^{3+}-Tb^{3+} (solid blue triangles). The solid lines are the linear fit curves.

Table 1: Parameters and linear fit of (2) for all Y_2O_3 samples.

Sample	ΔE (cm^{-1})	Linear fit
Y_2O_3:Er^{3+}	825.58	ln(FIR) = 2.80 + (−1187.89)/T
Y_2O_3:Er^{3+}-Eu^{3+}-Tb^{3+}	826.24	ln(FIR) = 2.79 + (−1188.84)/T
Y_2O_3:Er^{3+}-Tb^{3+}	801.77	ln(FIR) = 2.57 + (−1153.63)/T
Y_2O_3:Er^{3+}-Eu^{3+}	737.62	ln(FIR) = 2.46 + (−1061.33)/T

constant; and T is the thermodynamic temperature. It is worth mentioning that both preexponential factor and energy gap depend on the host crystalline structure and the dopant concentration [10, 18, 19]. Expression (1) can be linearized and its coefficients can be obtained if we apply the natural logarithm to both sides of that relation

$$\ln(\mathrm{FIR}) = \ln C - \frac{\Delta E}{kT}. \quad (2)$$

Figure 4 plots ln(FIR) versus T^{-1}. According to (2), the terms C and ΔE can be determined from the intercept and slope of the fittings, respectively. Table 1 summarizes the results, which will subsequently be used in Section 3.3 to estimate the internal temperature reached by the nanocrystals during the experiment with increasing power densities.

As can be noticed, the values of the preexponential factor C and the energy gap ΔE are not equal among the investigated samples, although the host crystalline phase and the erbium concentration remained the same. In particular, the obtained values for ΔE are in good agreement with previous works. The addition of Eu^{3+} and Tb^{3+} ions modified very little this quantity, as the relative errors calculated with respect to the reference value [17] are always smaller than 7.5%. Curiously, the sample doped simultaneously with Er^{3+}, Eu^{3+}, and Tb^{3+} presented an energy gap value very similar to the single-doped Y_2O_3 nanocrystals' sample. Similar behavior was previously reported for Er/Yb-doped $NaY(WO_4)_2$ nanocrystals [10].

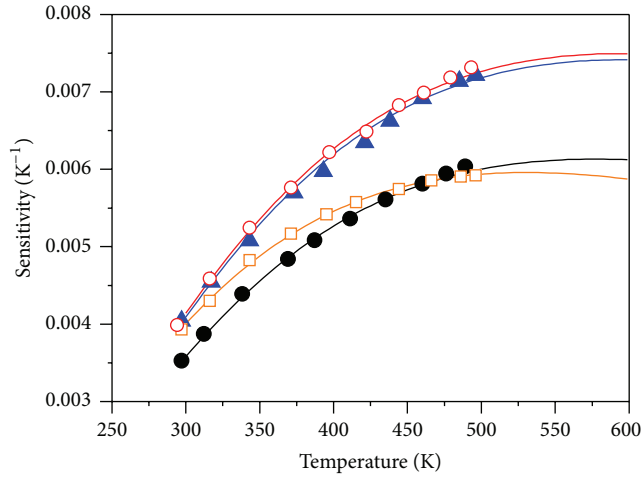

Figure 5: Sensitivity of Er^{3+} transitions ($^2H_{11/2} \rightarrow {}^4I_{15/2}$ and $^4S_{3/2} \rightarrow {}^4I_{15/2}$) as a function of temperature to our samples, Y_2O_3:Er^{3+} (open red circles), Y_2O_3:Er^{3+}-Tb^{3+} (solid black circles), Y_2O_3:Er^{3+}-Eu^{3+} (open orange squares), and Y_2O_3:Er^{3+}-Eu^{3+}-Tb^{3+} (solid blue triangles). The solid lines are the fit curves using (3).

From the obtained parameters (Table 1) we can also determine the sensitivity of the fluorescence intensity ratio (FIR) to temperature changes. The sensitivity (S) is defined as [18]

$$S = \frac{\partial(\mathrm{FIR})}{\partial T} = \mathrm{FIR} \cdot \left(\frac{\Delta E}{kT^2}\right). \quad (3)$$

Naturally, as both C and ΔE depend on the dopant concentration and host structure, the sensor sensitivity is also affected by these properties [10, 18, 19]. Moreover, the presence of Eu^{3+} and Tb^{3+} can provide extra channels to depopulate the erbium's emission levels by energy transfer mechanisms. Owing to this fact, the radiative spontaneous emission rate of codoped samples can be different from the Er^{3+}-doped nanocrystals, which is implied in distinct preexponential factors and sensors sensitivities [20].

Figure 5 plots the sensitivity versus temperature from the data obtained during temperature sensor calibration and also shows the curve fit based on (3) and the parameters from Table 1. As can be seen, different dopant ions result in slightly distinct sensitivity of the FIR.

From our experimental results, we believe that the presence of distinct ions modifies slightly the crystal field experienced by the Er^{3+} ions and alters the radiative spontaneous decay rate for the erbium emission levels. However, we could not identify the exact extent of this modification and the role of the pair Eu^{3+}/Tb^{3+} in the energy gap between the $^2H_{11/2}$ and $^4S_{3/2}$ erbium level's, as well as in the preexponential factor and the sensor sensitivities. A systematic investigation exploiting samples with different rare earth relative concentrations, but fixing the nanocrystals' morphology, must be undertaken in order to elucidate this issue. Nevertheless, such study is beyond the scope of the present work.

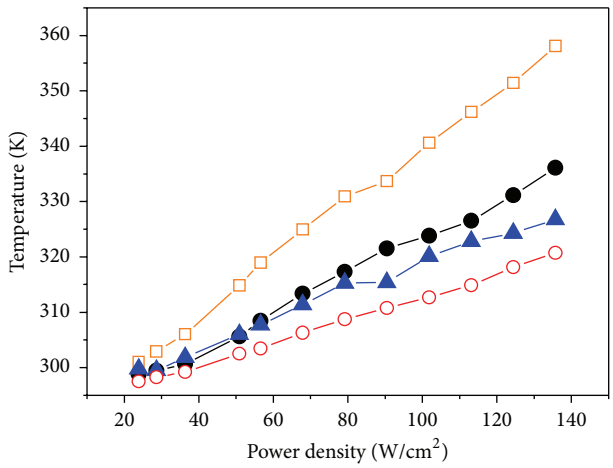

FIGURE 6: Optical heating behavior of the studied samples under 800 nm diode laser excitation as a function of pump power density, Y_2O_3:Er^{3+} (open red circles), Y_2O_3:Er^{3+}-Tb^{3+} (solid black circles), Y_2O_3:Er^{3+}-Eu^{3+} (open orange squares), and Y_2O_3:Er^{3+}-Eu^{3+}-Tb^{3+} (solid blue triangles).

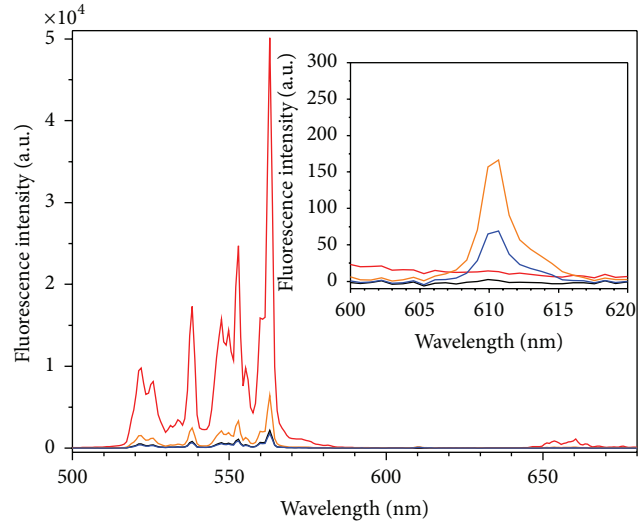

FIGURE 7: Upconversion emission spectra of Y_2O_3:Er^{3+} (red), Y_2O_3:Er^{3+}-Tb^{3+} (black), Y_2O_3:Er^{3+}-Eu^{3+} (orange), and Y_2O_3:Er^{3+}-Eu^{3+}-Tb^{3+} (blue) under 800 nm diode laser excitation with 500 mW laser power. The inset highlights the emission band at 611 nm.

3.3. Optical Heating Behavior. To determine the optical heating behavior of the samples, the emission bands around 523 nm and 551 nm of Er^{3+} were monitored and the FIR was determined, while the pump power density focused on the samples was adjusted from 23.9 W/cm^2 to 135.7 W/cm^2 (211 mW to 1200 mW pump power). Based on this data, the relations of Table 1 were used to estimate the temperature reached inside the nanoparticles.

The comparative graph of sample's heating is shown in Figure 6. As expected, the increase in power density resulted in optical heating with specific result for each group of nanoparticles. The internal heat generation through optical excitation in materials doped with rare earth ions is mainly due to nonradiative decay processes involving emission of phonons to the crystal lattice and subsequent heating. Another factor favoring the heating of nanoparticles is the quantum confinement of phonons that enhances the electron-phonon coupling thus promoting heat generation [15], this contribution should be the same for all our samples, and therefore the difference in doping is mainly responsible for the difference in heating behavior.

The sample doped only with Er^{3+} showed the lowest heating performance, with the temperature ranging from 297 K to 321 K, and the sample doped with Er^{3+}-Eu^{3+}-Tb^{3+} reached slightly higher temperature, ranging from 300 K to 327 K, while the sample doped with Er^{3+}-Tb^{3+} ranged from 299 K to 336 K. In its turn, the sample doped with Er^{3+}-Eu^{3+} showed the highest heating with temperature ranging from 301 K to 358 K for the same variation in pump power density (23.9 to 135.7 W/cm^2). As the results show, the multiple doping was effective, enabling the codoped samples to achieve higher temperature values under the same optical excitation in comparison to the Er^{3+}-doped particles.

Indeed, including more than one impurity ion in the samples, we favor energy transfer processes between ions. Therefore, a fraction of the energy absorbed predominantly by Er^{3+} ions, which play the role of sensitizers, could be transferred to the other ions, which creates other decay channels that include nonradiative processes. This assumption is corroborated comparing the upconverted luminescence spectra of all samples, presented in Figure 7. The addition of Tb^{3+} and Eu^{3+} ions depletes the intensity of the emitted light due to the erbium transitions. As the laser wavelength tuned at 800 nm cannot be absorbed directly by the Eu^{3+} and Tb^{3+} ions, the reduction in the erbium emission should be associated with the energy transfer from erbium to the other rare earth ions present in the samples.

From the experimental results, we believe that the presence of Tb^{3+} ions increases the optical heating process due to the energy transfer mechanism between the $^4I_{13/2}$ erbium level and the terbium $^7F_0$ level [21]. Due to this process, the excitation of $^2H_{11/2}$ and $^4S_{3/2}$ is reduced. The Tb^{3+} ions excited at the $^7F_0$ level decay nonradiatively to the other ^7F_j, transferring this energy to the host, which increases the Y_2O_3:Er^{3+}-Tb^{3+} temperature at a higher amount than the single-doped erbium sample under the same optical excitation.

For the sample codoped with erbium and europium ions, more than one energy transfer mechanism can take place. As we detected a luminescence centered at 611 nm, related to the $^5D_0 \rightarrow {}^7F_2$ levels of Eu^{3+}, and the erbium emission presented quenching, probably energy has been transferred from erbium ions excited at the $^2H_{9/2}$, $^4F_{3/2}$, $^4H_{5/2}$, $^4F_{7/2}$, $^2H_{11/2}$, and $^4S_{3/2}$ levels to the ^5D_j levels of Eu^{3+}. Besides, phonon-assisted energy transfer in Er^{3+} excited at $^4I_{11/2}$ and $^4I_{13/2}$ to the ^7F_j levels of Eu^{3+} is also probable [22, 23]. The Eu^{3+} ions excited at the ^7F_j levels decay nonradiatively to the ground state, heating up the Y_2O_3 nanocrystals. We believe that this sample presented the best optical heating

performance among the investigated materials in this work, owing to the several nonradiative decays and phonon-assisted energy transfer mechanisms involved in this process.

A more complex analysis must be made in order to understand the optical heating behavior of the Y_2O_3:Eu^{3+}-Er^{3+}-Tb^{3+} sample. Despite the fact that all proposed energy transfer mechanisms for the Y_2O_3:Eu^{3+}-Er^{3+} and Y_2O_3:Er^{3+}-Tb^{3+} are involved in this case, a highly probable energy transfer from Tb^{3+} to Eu^{3+} can also take place [24]. Hence, we believe that the presence of the three ions species creates a competition mechanism, in which Tb^{3+} and Eu^{3+} ions compete to receive energy from the excited erbium ions. Additionally, most of the energy absorbed by Tb^{3+} is transferred directly to Eu^{3+}, creating an alternative excitation path to the europium ions. Thus, only part of the Eu^{3+} ions are excited by the phonon-assisted energy transfer from Er^{3+} ions. As a result, the competition mechanisms between the three rare earth species in the Y_2O_3 samples result in a lower emission of phonons in comparison with the Y_2O_3:Eu^{3+}-Er^{3+} and Y_2O_3:Er^{3+}-Tb^{3+} samples, resulting in weaker heating under the same optical excitation. A more detailed investigation of energy transfer mechanisms between the ions in our samples is beyond the scope of this work. Although several mechanisms had been proposed [23, 25, 26], to the best of our knowledge, none of them deeply analyzed the influence of these mechanisms on the optical heating behavior.

4. Conclusion

Nanoparticles of Y_2O_3 doped with Er^{3+}, Eu^{3+}, and Tb^{3+} were synthesized by PVA-assisted sol-gel route, and their structural characterization was carried out. The doping with Er^{3+} was effective in sensitizing the nanoparticles to the excitation wavelength of 800 nm from a CW diode laser, allowing us to analyze the FIR of the upconversion bands of the Er^{3+} levels $^2H_{11/2}$ and $^4S_{3/2}$. From this point, we calibrated an optical thermometer and used the codoping with Eu^{3+} and Tb^{3+} ions to allow the nanoparticles to achieve higher temperatures under the same optical excitation in comparison to the values obtained using Er^{3+}-doped nanocrystals. The effect of dopants on the temperature sensitivity of the FIR was also determined. The power densities used, as well as the temperatures reached by the samples, are in the regions commonly used in hyperthermia treatments, indicating that these particles can be promising alternatives for this kind of treatment when an 800 nm CW excitation is convenient.

Conflict of Interests

The authors declare that there is no conflict of interests regarding the publication of this paper.

Acknowledgments

The authors thank the financial support from CAPES, CNPq/MCT, FAPITEC/SE, Nanofoton Network, and INCT-FOTÔNICA.

References

[1] R. R. Anderson and J. A. Parrish, "The optics of human skin," *Journal of Investigative Dermatology*, vol. 77, no. 1, pp. 13–19, 1981.

[2] A. Smith M, M. Mancini C, and S. Nie, "Bioimaging: second window for in vivo imaging," *Nature Nanotechnology*, vol. 4, pp. 710–711, 2009.

[3] D. Jaque and C. Jacinto, "Luminescent nanoprobes for thermal bio-sensing: towards controlled photo-thermal therapies," *Journal of Luminescence*, 2015.

[4] D. K. Chatterjee, A. J. Rufaihah, and Y. Zhang, "Upconversion fluorescence imaging of cells and small animals using lanthanide doped nanocrystals," *Biomaterials*, vol. 29, no. 7, pp. 937–943, 2008.

[5] O. A. Savchuk, P. Haro-González, J. J. Carvajal et al., "Er:Yb:NaY_2F_5O up-converting nanoparticles for sub-tissue fluorescence lifetime thermal sensing," *Nanoscale*, vol. 6, no. 16, pp. 9727–9733, 2014.

[6] R. Dey, A. Pandey, and V. K. Rai, "Er^{3+}-Yb^{3+} and Eu^{3+}-Er^{3+}-Yb^{3+} codoped Y_2O_3 phosphors as optical heater," *Sensors and Actuators B: Chemical*, vol. 190, pp. 512–515, 2014.

[7] M. K. Mahata, K. Kumara, and V. K. Rai, "Er^{3+}–Yb^{3+} doped vanadate nanocrystals: a highly sensitive thermographic phosphor and its optical nanoheater behavior," *Sensors and Actuators B: Chemical*, vol. 209, pp. 775–780, 2015.

[8] A. Pandey, V. K. Rai, V. Kumar, V. Kumar, and H. C. Swart, "Upconversion based temperature sensing ability of Er^{3+}–Yb^{3+} codoped $SrWO_4$: an optical heating phosphor," *Sensors and Actuators B: Chemical*, vol. 209, pp. 352–358, 2015.

[9] A. K. Soni, R. Dey, and V. K. Rai, "Stark sublevels in Tm^{3+}–Yb^{3+} codoped $Na_2Y_2B_2O_7$ nanophosphor for multifunctional applications," *RSC Advances*, vol. 5, no. 44, pp. 34999–35009, 2015.

[10] H. Zheng, B. Chen, H. Yu et al., "Temperature sensing and optical heating in Er^{3+} single-doped and Er^{3+}/Yb^{3+} codoped $NaY(WO_4)_2$ particles," *RSC Advances*, vol. 4, pp. 47556–47563, 2014.

[11] E. Hemmer, N. Venkatachalam, H. Hyodo et al., "Upconverting and NIR emitting rare earth based nanostructures for NIR-bioimaging," *Nanoscale*, vol. 5, no. 23, pp. 11339–11361, 2013.

[12] U. Rocha, K. U. Kumar, C. Jacinto et al., "Nd^{3+} doped LaF_3 nanoparticles as self-monitored photo-thermal agents," *Applied Physics Letters*, vol. 104, no. 5, Article ID 053703, 2014.

[13] A. Bednarkiewicz, D. Wawrzynczyk, M. Nyk, and W. Strek, "Optically stimulated heating using Nd^{3+} doped $NaYF_4$ colloidal near infrared nanophosphors," *Applied Physics B*, vol. 103, no. 4, pp. 847–852, 2011.

[14] D. Jaque, L. Martínez Maestro, B. del Rosal et al., "Nanoparticles for photothermal therapies," *Nanoscale*, vol. 6, no. 16, pp. 9494–9530, 2014.

[15] B. D. Cullity, *Elements of X-Ray Diffraction*, Addison-Wesley, Reading, Mass, USA, 1978.

[16] M. A. Gomes, M. E. G. Valerio, and Z. S. Macedo, "Particle size control of Y_2O_3:Eu^{3+} prepared via a coconut water-assisted sol-gel method," *Journal of Nanomaterials*, vol. 2011, Article ID 469685, 6 pages, 2011.

[17] V. K. Tikhomirov, K. Driesen, V. D. Rodriguez, P. Gredin, M. Mortier, and V. V. Moshchalkov, "Optical nanoheater based on the Yb^{3+}-Er^{3+} co-doped nanoparticles," *Optics Express*, vol. 17, no. 14, pp. 11794–11798, 2009.

[18] S. F. León-Luis, U. R. Rodríguez-Mendoza, I. R. Martín, E. Lalla, and V. Lavín, "Effects of Er^{3+} concentration on thermal sensitivity in optical temperature fluorotellurite glass sensors," *Sensors and Actuators B: Chemical*, vol. 176, pp. 1167–1175, 2013.

[19] S. F. León-Luis, U. R. Rodríguez-Mendoza, P. Haro-González, I. R. Martín, and V. Lavín, "Role of the host matrix on the thermal sensitivity of Er^{3+} luminescence in optical temperature sensors," *Sensors and Actuators B: Chemical*, vol. 174, pp. 176–186, 2012.

[20] M. Quintanilla, E. Cantelar, F. Cussó, M. Villegas, and A. C. Caballero, "Temperature sensing with up-converting submicron-sized $LiNbO_3$:Er^{3+}/Yb^{3+} particles," *Applied Physics Express*, vol. 4, no. 2, Article ID 022601, 2011.

[21] L. G. Van Uitert, E. F. Dearborn, and J. J. Rubin, "Mechanisms of energy transfer involving trivalent Er and Tb or Tm in sodium rare-earth tungstates," *The Journal of Chemical Physics*, vol. 47, no. 9, pp. 3653–3661, 1967.

[22] J. Yang, L. Zhang, L. Wen, S. Dai, L. Hu, and Z. Jiang, "Comparative investigation on energy transfer mechanisms between Er^{3+} and Ce^{3+} (Eu^{3+}, Tb^{3+}) in tellurite glasses," *Chemical Physics Letters*, vol. 384, no. 4-6, pp. 295–298, 2004.

[23] J. Wang, Y. Zhou, S. Dai, T. Xu, and Q. Nie, "State-selective energy transfer from Er^{3+} to Eu^{3+} in Bi_2O_3-GeO_2-Ga_2O_3-Na_2O glasses," *Spectrochimica Acta A*, vol. 72, no. 1, pp. 41–45, 2009.

[24] G. A. Sotiriou, M. Schneider, and S. E. Pratsinis, "Color-tunable nanophosphors by codoping flame-made Y_2O_3 with Tb and Eu," *Journal of Physical Chemistry C*, vol. 115, no. 4, pp. 1084–1089, 2011.

[25] L. G. Van Uitert and L. F. Johnson, "Energy transfer between rare–earth ions," *The Journal of Chemical Physics*, vol. 44, no. 9, pp. 3514–3522, 1966.

[26] T. Anh, P. Benalloul, C. Barthou, L. T. Giang, N. Vu, and L. Minh, "Luminescence, energy transfer, and upconversion mechanisms of Y_2O_3 nanomaterials doped with Eu^{3+}, Tb^{3+}, Tm^{3+}, Er^{3+}, and Yb^{3+} ions," *Journal of Nanomaterials*, vol. 2007, Article ID 48247, 10 pages, 2007.